Hindawi
Advances in Materials Science and Engineering
Volume 2019, Article ID 3079393, 8 pages
https://doi.org/10.1155/2019/3079393

Research Article

Understanding the Preferred Crystal Orientation of Sputtered Silver in Ar/N_2 Atmosphere: A Microstructure Investigation

YuHao Hu,[1] Jiajun Zhu,[1,2] Chao Zhang,[3] Wulin Yang,[1,2] Licai Fu,[1,2] Deyi Li,[1,2] and Lingping Zhou[1,2]

[1]*College of Materials Science and Engineering, Hunan University, Changsha 410082, China*
[2]*Hunan Province Key Laboratory for Spray Deposition Technology and Application, Hunan University, Changsha 410082, China*
[3]*Science and Technology on Power Sources Laboratory, Tianjin Institute of Power Sources, Tianjin 300384, China*

Correspondence should be addressed to Jiajun Zhu; jiajun@hnu.edu.cn and Chao Zhang; zcmaster@163.com

Received 9 May 2019; Accepted 9 July 2019; Published 6 November 2019

Academic Editor: Pramod Koshy

Silver thin films were prepared by direct current (DC) magnetron sputtering technique in Ar/N_2 atmosphere with various N_2 volumetric ratios on Si substrates. Silver thin films prepared in pure Ar atmosphere show highly (111) preferred orientation. However, as the N_2 content increases, Ag (111) preferred orientation evolves into (100) preferred orientation gradually. When N_2 content is more than 12.5 vol.%, silver thin films exhibit highly (100) preferred orientation. Moreover, the average grain size decreases with increasing N_2 content. Silver thin films with low relative density are prepared at high N_2 content, which results in higher resistivity of films. By analyzing the resistivity and microstructures of silver thin films, the optimum range of N_2 content to get compact silver thin films is found to be not more than 33.3 vol.%. Finally, the mechanism of N_2 addition on microstructure evolution of silver thin films was proposed.

1. Introduction

Noble metal silver (Ag) has excellent characteristics, such as low electrical resistivity, high thermal conduction, high reflectivity in visible and infrared regions, and great weldable and antimicrobial properties [1–3]. Silver and corresponding composites are widely used in the fields of electronics, aerospace, medical instruments, etc. For example, Ag/GaN multilayer films are used as the conductor electrodes of light-emitting diodes (LEDs), the coatings of laser safety glasses, and display window materials which block microwave radiation [4, 5]. Ag/TiN or Ag/TaN multilayer films are potential materials to be used as interconnects on integrated circuits [6–8]. Beyond that, Ag/TiN multilayer films are also used in the photocatalytic field [9].

In the above applications, the silver thin films were generally prepared by physical vapor deposition (PVD) in Ar atmosphere while nitride thin films were prepared by PVD in Ar/N_2 atmosphere. During the preparation process of Ag/nitride multilayer films, the sputtering gas needed to be changed; thus, the preparation process of Ag/nitride multilayer films was complicated. If the Ag/nitride multilayer films can be prepared in the same Ar/N_2 atmosphere, it will simplify the preparation process of Ag/nitride multilayer thin films. Therefore, it is necessary to study the influence of Ar/N_2 sputtering gas on microstructures of silver thin films.

Compared with Ar, N_2 exhibits higher chemical reactivity. It is difficult to obtain pure metal thin films in N_2 or Ar/N_2 atmospheres. Hence, N_2 is usually used to prepare nitride thin films via PVD (physical vapor deposition). Moreover, the influence of N_2 content in Ar/N_2 atmosphere on crystal orientation, grain size, and relative density of films is also demonstrated in previous research studies. In 2004, Kawamura et al. reported that the Ni thin films were prepared in low N_2 flow ratio; however, Ni_3N phase was observed when the flow ratio of N_2 arrived to 12%. Furthermore, the crystal orientation of Ni thin films was changed from (111) to (100) due to the introduction of N_2 into the sputtering atmosphere [10]. Afterwards, they discovered that the intensity of (002) peak (C-axis orientation)

of Ru thin films decreased with the increasing N_2 sputtering gas proportion at a substrate temperature of 100°C, and the intensity of (002) peak of Ru thin films eventually disappeared when the N_2 content was 50% flow ratio. In addition, it was observed by Auger electron spectroscopy that the Ru film deposited at 50% N_2 content contained nitrogen [11]. Calinas et al. developed the formation of nanocrystalline copper thin films through controlled addition of nitrogen. According to their work, the average nitrogen content for the Cu-N thin films was found to be 1.5 at.%, 3.5 at.%, and 7 at.% for the samples with $P_{N2}:P_{Ar}$ ratios of 1:60, 1:30, and 1:2, respectively. And, the Cu_3N phase was identified with the highest $P_{N2}:P_{Ar}$ ratio of 1:2. Moreover, when the nitrogen content in Cu thin films was low, the grain size of Cu thin films rapidly decreased with the increase of the nitrogen content [12]. Based on all above mentioned, the N_2 content has a significant influence on the microstructures and composition of metal thin films; however, the microstructures of silver thin films prepared at various N_2 contents in Ar/N_2 atmosphere are rarely reported. Thus, it is meaningful to research the effect of N_2 content in Ar/N_2 atmosphere on the microstructures of silver thin films and find a suitable range of N_2 content to prepare silver thin films.

In this paper, a series of samples were prepared by direct current (DC) magnetron sputtering in Ar/N_2 atmosphere with various N_2 contents (0 vol.%, 8 vol.%, 12.5 vol.%, 33.3 vol.%, 50 vol.%, 66.7 vol.%, and 100 vol.%) on Si substrates. Crystal orientation, texture coefficient, and grain size of silver thin films were characterized as a function of N_2 content. Furthermore, surface morphology, cross-sectional morphology, and electrical properties of silver thin films were investigated. In the end, the mechanism of microstructure evolution was also proposed.

2. Experimental

Silver thin films were prepared by direct current magnetron sputtering deposition system (MIS800). (100) single crystal silicon sheets were selected as the substrate material and cut into square-shaped of approximately $10\,\text{mm} \times 10\,\text{mm} \times 0.38\,\text{mm}$. These Si specimens were ultrasonically cleaned with acetone, ethanol, and deionized water in sequence before being dried. Prior to deposition, the base pressure was less than 4.0×10^{-4} Pa. Then, the substrates were cleaned by Ar^+ beam bombardment with 600 V/50 mA lasting for 10 minutes to remove surface impurity. The substrate holder was then rotated to be perpendicular to the direction parallel with the Ag target (99.99% purity). During the deposition, the distance between Ag target and substrate was 70 mm. The working pressure was maintained at 1 Pa, and the power was 120 W. Finally, the films were deposited for 10 minutes at various N_2 contents in Ar/N_2 atmosphere. The samples numbered on the basis of N_2 content are shown in the Table 1.

The phase composition and crystallographic structure of silver thin films were analyzed by X-ray diffraction (XRD) measurement (MiniFlex made by Rigaku) with Cu K-α radiation source. Surface and cross-sectional morphologies of silver thin films were recorded by using a scanning electron microscope (SEM, Hitachi S-4800). The surface chemical compositions of the silver thin films were studied by the K-ALPHA X-ray (Thermo Fisher Scientific) photoelectron spectroscopy (XPS) instrument. The sheet resistance of silver thin films on Si substrates was measured by a four-point probe (RTS-8). The resistivity was calculated according the following formula:

$$\rho = R_s d, \tag{1}$$

where d is the thickness of the film measured by SEM and R_s is the sheet resistance of the film.

3. Results and Discussion

3.1. Crystal Orientation of Silver Thin Films. Figure 1 shows X-ray diffraction patterns of silver thin films on Si substrates. The value of ordinate was set same in order to compare the Ag peak intensity of all samples easily. In Figure 1, high Ag (111) and (200) diffraction peaks are found clearly in all samples. The Si substrate peak is so high that Ag (220), (311), and (222) diffraction peaks could not be observed in almost all samples.

The phase of nitride is not detected by XRD, which is in accordance with the results of XPS spectra that are shown in Figure 2. Considering all the samples were exposed in air before XPS characterization, the sample was etched 5 minutes by Ar^+ (2 keV) to exclude the absorptions of C, N, and O elements from the air. As seen from the wide-scan spectra of S0, S33, and S100 in Figure 2(a), only Ag is observed. The high-resolution spectra of Ag 3d and the corresponding fitting curves are shown in Figure 2(b), the area ratio of the Ag $3d_{3/2}$ and Ag $3d_{5/2}$ peaks is about 2/3, and the binding energy of Ag $3d_{3/2}$ and Ag $3d_{5/2}$ is 374.4 eV and 368.4 eV, respectively, which agrees with the binding energy of metallic Ag [13, 14]. Based on the results of XRD and XPS, no nitride and oxide exist in the thin film, and pure silver thin films were obtained in pure N_2 atmosphere.

It is clear that the relative intensities of Ag (111) and (200) diffraction peaks are different for silver thin films prepared at different N_2 contents in Figure 1. Preferred orientation exists in all samples. In order to explain the degree of the silver thin films' preferred orientation, the texture coefficients of (111) plane and (100) plane ($P_{(111)}$ and $P_{(100)}$) were represented quantitatively by the Harris method in the following formula [15, 16]:

$$P_{(\text{hkl})_i} = \frac{I_{(\text{hkl})_i}}{I_{0\,(\text{hkl})_i}} \left[\frac{1}{n} \sum_{1}^{n} \frac{I_{(\text{hkl})_i}}{I_{0\,(\text{hkl})_i}} \right]^{-1}, \tag{2}$$

where $I_{0(\text{hkl})i}$ is the standard intensity of the (hkl) plane for the ith peak from powder diffraction file (PDF) card, $I_{(\text{hkl})i}$ is the detected intensity of the (hkl) plane for the ith peak, and n is the total number of diffraction peaks considered in the analysis. ICSD card no. 04-0783 of Ag was used in this calculation, and other peaks were so weak that only (111) and (200) peaks were considered. The values of $P_{(111)}$ and $P_{(100)}$ of silver thin films on Si substrates depending upon the N_2 content are shown in Figure 3 ($P_{(111)} + P_{(100)} = 2$). The value of $P_{(100)}$ suddenly increases when the N_2 content changes from 0 vol.% to 12.5 vol.% and slightly increases with the increasing N_2 content ranging from 12.5 vol.% to 33.3 vol.%. When N_2 content exceeds 33.3 vol.%, $P_{(100)}$

Table 1: Ar/N_2 ratio and numbered messages.

N_2 content (volumetric ratio)	0%	8%	12.5%	33.3%	50%	66.7%	100%
Sample number	S0	S8	S12	S33	S50	S66	S100

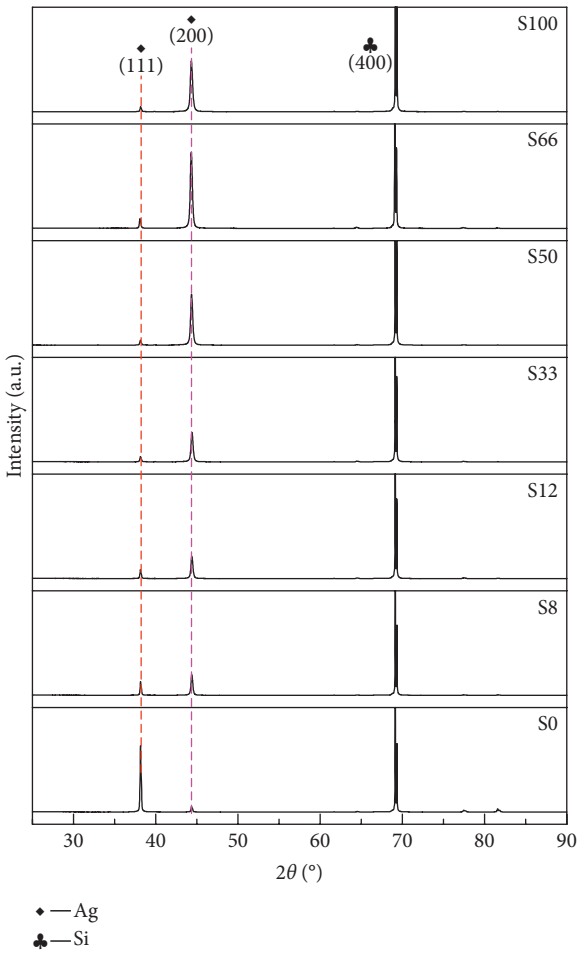

Figure 1: X-ray diffraction patterns (XRD) of silver thin films (S0, S8, S12, S33, S50, S66, and S100).

becomes stable. Overall, as the N_2 content increases, grains prefer to grow along (100) plane while (111) plane is restrained. Based on the above results, silver thin films with highly (111) preferred orientation were prepared in pure Ar atmosphere ($P_{(111)} = 1.66 >> 1$), and silver thin films with highly (100) preferred orientation were prepared at 12.5 vol.% N_2 content ($P_{(100)} = 1.72 >> 1$). Therefore, it is concluded that the preferred orientation of silver thin films can be adjusted successfully in Ar/N_2 atmosphere through controlling the N_2 content.

3.2. Grain Size of Silver Thin Films. The grain sizes of (111) plane ($G_{(111)}$) and (200) plane ($G_{(200)}$) were calculated based on the Scherrer formula:

$$G = \frac{k\lambda}{\beta \cos\theta}, \tag{3}$$

where G is the grain size, $k = 0.89$, $\lambda = 0.154056$ nm, β is the full width at half maximum (FWHM) of the diffraction peak, and θ is the Bragg angle at corresponding diffraction peak. The instrument width was deducted by Si standard samples. $\overline{G}$ represents the average grain size of silver thin films, which were estimated according to the following formula:

$$\overline{G} = \frac{G_{(111)}P_{(111)} + G_{(200)}P_{(100)}}{2}. \tag{4}$$

Grain size of silver thin films is shown in Figure 4. It is obvious that $G_{(111)}$ is bigger than $G_{(200)}$ for all samples, and $G_{(111)}$ decreases with increasing N_2 content. The average grain size $\overline{G}$ decreases rapidly from 82 nm to 40 nm with the increasing N_2 content ranging from 0 vol.% to 12.5 vol.%, and then it decreases slightly. Finally, $\overline{G}$ reduces to 31 nm when the N_2 content is 100%. The results of grain size suggest that grain growth was suppressed in N_2 atmosphere during the deposition.

3.3. Surface and Cross-Sectional Morphologies of Silver Thin Films. The SEM cross-sectional images of S0, S12, S33, S50, and S100 are shown in Figure 5. The cross-sectional structure of silver thin films is compact as shown in Figure 5(a). Denser structure is also observed in Figure 5(b). However, few holes are observed in S33 in Figure 5(c). Compared with S33, a large number of holes exist in S50 and S100 in Figures 5(d) and 5(e), and the mean diameter of holes in S50 and S100 is bigger than that in S33. The porous-style structure indicates the low relative density of films; thus, the relative densities of S50 and S100 are extremely worse than S33. In addition, the thickness of silver thin films decreases from 1.9 μm to 1.6 μm when the N_2 content ranged from 0 vol.% to 33.3 vol.%, which suggests that the deposition rate of silver thin films decreases with increasing N_2 content. However, the thickness of silver thin films prepared at 50 vol.% N_2 content is 1.8 μm. Compared to S33, the increase of thickness in S50 may be caused by its loose structure. Although the structure in S100 is loose, the thickness of S100 reduces to 1.45 μm, so a very low deposition rate existed in pure N_2 atmosphere. In summary, as N_2 content increases, the thickness of films decreases firstly, then increases, and decreases finally.

The SEM surface images of S0, S12, S33, S50, and S100 are shown in Figure 5. Clean and flat surface can be observed in S0, S12, and S33 in Figures 5(a1), 5(b1), and 5(c1). The average surface granule size of S0, S12, and S33 decreases in sequence. The relative flat surface in S50 is also observed in Figure 5(d1); however, many holes and a few big spherical crystalline granules are observed on the surface. In Figure 5(e1), spherical crystalline granules are dispersed on the surface, and a lot of holes and grooves exist. It is obvious that the surface of S100 is extremely sparser and rough. The morphology can indirectly reflect the relative density of films. According to the analysis of surface and cross-sectional morphologies, the relative density of films was evaluated. The sequence of films' relative density from high to

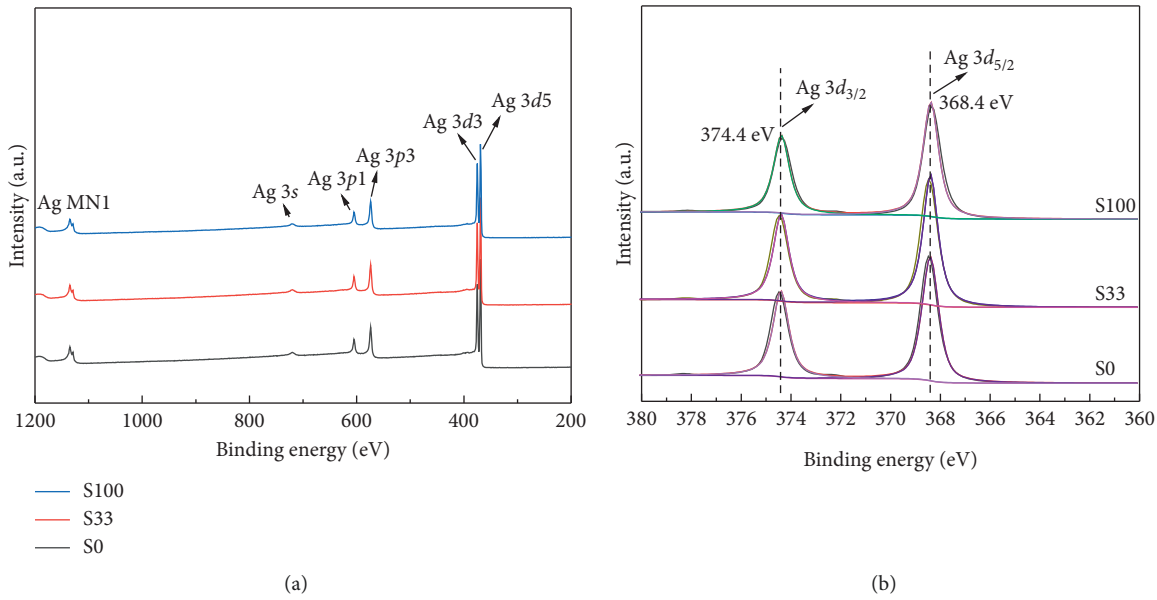

FIGURE 2: XPS spectra of S0, S33, and S100. (a) The wide-scan spectra of S100 sample. (b) Ag 3*d* spectra.

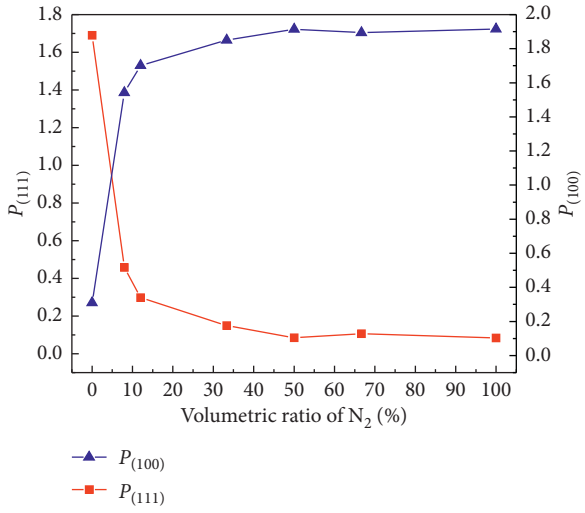

FIGURE 3: $P_{(111)}$ and $P_{(100)}$ of silver thin films on Si substrates as a function of the volumetric ratio of N_2 content.

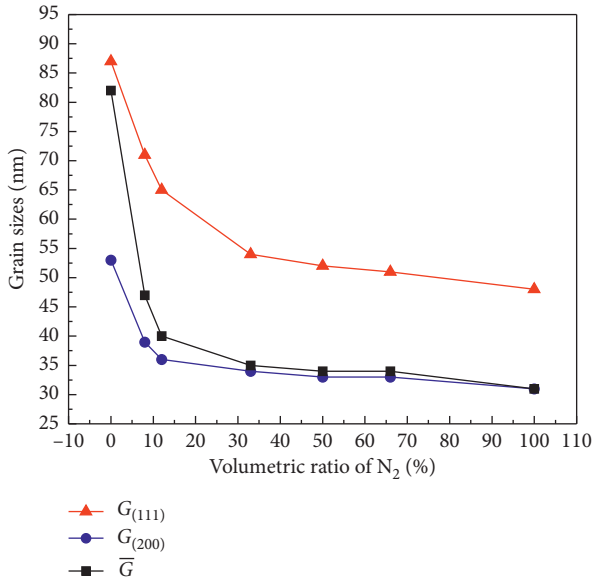

FIGURE 4: Grain size of silver thin films as a function of the volumetric ratio of N_2 content.

low is as follows: S0 and S12, S33, S50, and S100, which indicates that the high N_2 content in Ar/N_2 atmosphere resulted in the low relative density of films during the deposition. Therefore, to obtain a compact silver thin film through PVD process in Ar/N_2 atmosphere, the N_2 content does not exceed 33.3 vol.%.

3.4. Resistivity of Silver Thin Films. The resistivity of silver thin films is shown in Figure 6. It can be seen from the figure that the resistivity of silver thin films increased with increasing N_2 content until the N_2 content reached 66.7 vol.%, and then the resistivity of silver thin films stabilized with increasing N_2 content. Generally, the resistivity of metal thin films is the collaborative results of surface scattering, defects and impurity scattering, and grain boundary scattering. When the thickness of metal thin films is comparable in magnitude with the electronic mean free path of bulk material, the resistivity of metal thin films increases as the thickness of films decreases due to the surface scattering, which has been demonstrated by the Fuchs-Sondheimer (FS) model [17, 18]. However, the thicknesses of silver thin films in this study ranges from 1.45 μm to 1.9 μm, and it is extremely higher than the mean free path of electron (52 nm) [19]. Thus, the effect of films thickness on the resistivity can be negligible.

The resistivity of silver thin films prepared in pure Ar atmosphere is close to the resistivity of bulk material (1.6 $\mu\Omega$·cm). As the N_2 content increases from 0 vol.% to 33.3 vol.%, the resistivity of silver thin films increases slightly,

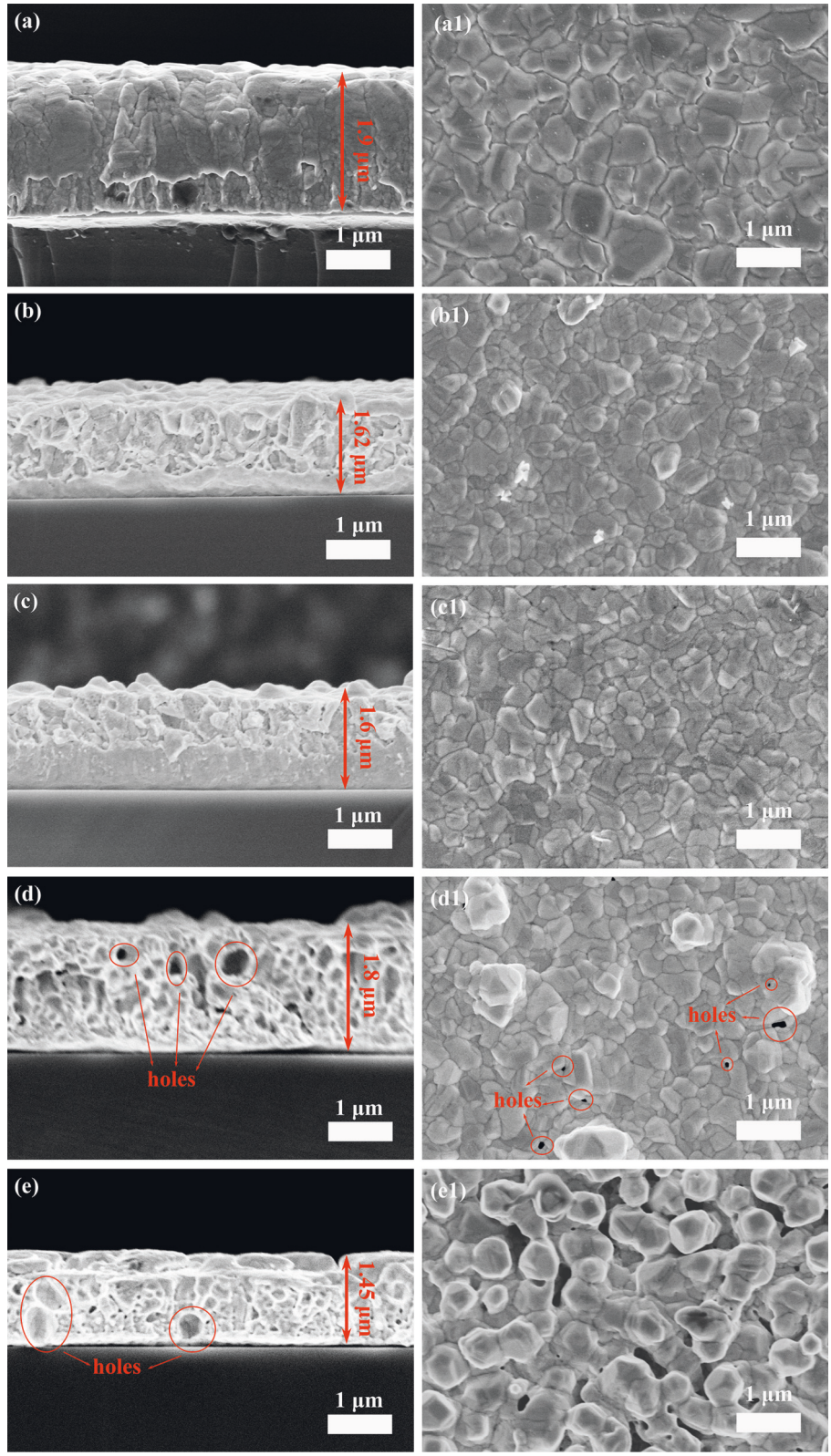

Figure 5: Surface and cross-sectional morphologies of S0, S12, S33, S50, and S100. (a), (b), (c), (d), and (e) show the cross-sectional morphologies of S0, S12, S33, S50, and S100, respectively. (a1), (b1), (c1), (d1), and (e1) show the surface morphologies of S0, S12, S33, S50, and S100, respectively.

while the average grain size of silver thin films decreases from 82 nm to 35 nm. The grain size is comparable with the mean free path of electron in our works. The famous Mayadas and Shatzkes (MS) model explained the relation between grain boundary and resistivity, and the MS model is shown as follows:

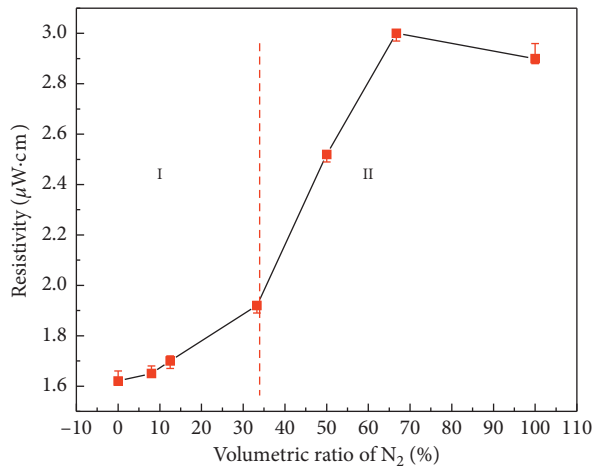

Figure 6: Resistivity of silver thin films as a function of the volumetric ratio of N_2 content.

$$\rho = \rho_0\left[1 + \frac{3}{2} \times \frac{1}{G} \times \frac{R}{1-R}\right], \tag{5}$$

where G is the grain size, R is the grain boundary reflection coefficient, ρ_0 is the bulk resistivity, and ρ is the measured resistivity. The amount of grain boundary per unit volume increases with the reduction of grain size. The grain boundary prevents the electron or phonon to transport, which leads to the increase of resistivity. Therefore, in phase I as shown in Figure 6, the main factor leading to the increasing resistivity of silver thin films is the grain boundary scattering. When the N_2 content exceeds 33.3 vol.%, the average grain size of silver thin films decreases from 40 nm to 31 nm slowly, so the resistivity caused by grain boundary scattering is close. When the N_2 content exceeds 33.3 vol.%, the relative density of films is low, and loose and porous structure can be observed from the surface and cross-sectional morphologies in Figure 5. The holes in films seriously hinder the transmission of electrons; thus, the defect scattering plays a major role in the dramatic increase in resistivity of films. In region II, the number of defects such as holes increases with increasing N_2 content; however, the number of defects no longer increases while the N_2 content arrived at 66.7 vol.%. Correspondingly, the resistivity of silver thin films increases rapidly, and then the resistivity of silver thin films stabilizes. As we all know, the quality of silver thin films can be estimated facilely by the resistivity of silver thin film. When the N_2 content ranges from 0 vol.% to 33.3 vol.%, the grain boundary scattering is the main reason to lead to a small difference in resistivity, and the effect of defect scattering on resistivity is similar, so the relative density of silver thin films is close. When the N_2 content exceeds 33.3 vol.%, the higher resistivity indicates that silver thin films have a lower relative density.

3.5. Mechanism of Microstructure Evolution. The crystal orientation, grain size, morphology, and relative density of silver thin films changed with the increasing N_2 content. So, the N_2 content has a significant effect on the microstructures of silver thin films. It can be speculated that the change in microstructures of silver thin films was related to the process of generation, transport, and deposition of sputtered particles. The schematic diagram of silver thin films' sputtering, transport, and deposition in pure Ar and pure N_2 atmospheres is described, respectively, in Figure 7.

During the complicated deposition process of silver thin films, the discharge is maintained by sputtering gas. In Ar/N_2 discharge, Ar^+ and $N_2{}^+$ are the main ions, and Ar atoms, N_2 molecules, and a small amount of N^+ ion also exist in the vacuum, which have been detected by plasma diagnostic techniques in some literatures [20–22]. There is no doubt that Ar^+ is the main ion in Ar discharge, and $N_2{}^+$ is the main ion in N_2 discharge. The electron density and ion density in Ar discharge are higher than those in N_2 discharge under other same parameters, which have been reported in literatures [20, 23]. A higher ionization rate of gas exists in Ar discharge compared with that in N_2 discharge, and a large quantity of sputtered Ar^+ result in high sputter yields in Ar discharge, so bigger and more Ag clusters exist in Ar compared with those in N_2. Moreover, another role of sputtering gas is to affect the energy distribution through the collision process with sputtered particles in the transport process of sputtered particles. Mean free path (λ) was estimated according to the following formula:

$$\lambda = \frac{kT}{\sqrt{2}\pi d^2 P}, \tag{6}$$

where k is the Boltzmann constant, T is the absolute temperature (298 K is adopted here), d is the molecular diameter, and P is the working pressure (1 Pa). The molecular diameter of Ar (3.4 Å) is smaller than N_2 (3.64 Å); thus, the mean free path of N_2 (λ_{N_2} is about 7 mm) is lower than Ar (λ_{Ar} is about 8 mm). When sputtered particles are transported from target to substrates, the sputtered particles are disturbed due to the collision with sputtering gas molecules. The collision frequency between sputtered particles and sputtering gas molecules is more intense in N_2 sputtering gas due to the low mean free path. Compared with Ar discharge, the higher collision frequency in the transport process and lower sputter yields led to a lower deposition rate in N_2 discharge, which is directly reflected in the thickness of silver thin films. Moreover, the high collision frequency in N_2 discharge leads to severe energy loss during the transport process. So, Ag clusters have lower energy E_k in N_2 discharge than that in Ar discharge when they arrived to substrates.

The carrying energy of Ag clusters is the driving force for migration and diffusion, and Ag clusters have higher energy E_k in Ar discharge; therefore, the Ag clusters are able to move to the gap among the clusters due to higher migration and diffusion, which result in a close-packed growth model of Ag clusters during the deposition. The close-packed plane of FCC metal is (111) plane, and grain growth of (111) plane is promoted. Compared with Ar discharge, the Ag clusters in N_2 discharge have lower energy. Ag clusters with lower mobility and diffusion tend to hold the initial position after they deposit on the substrates, so a relative loose-packed growth model of Ag clusters exists in N_2 discharge, which is

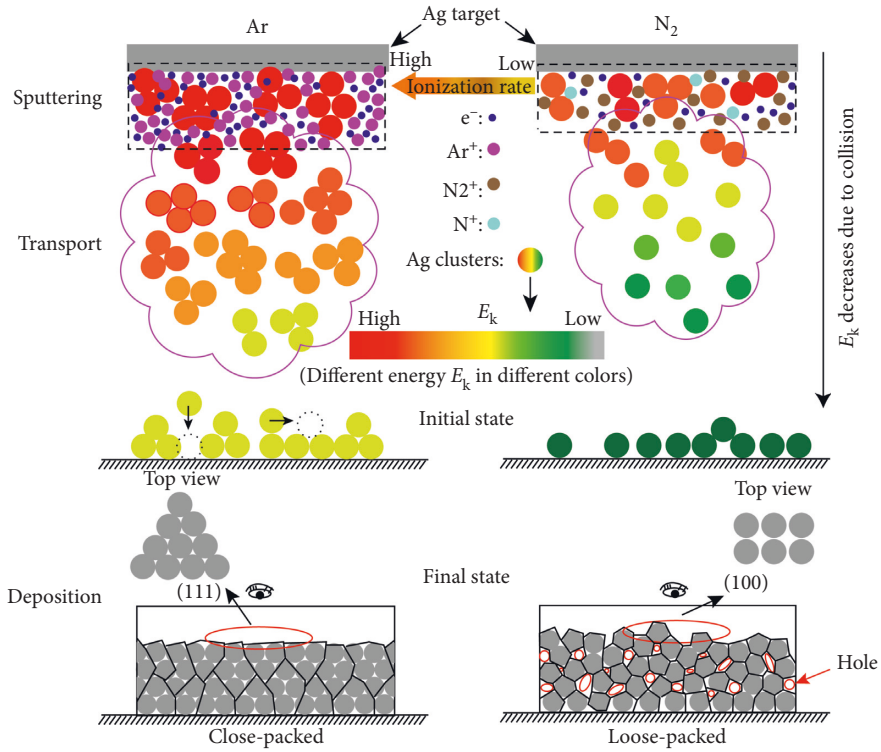

Figure 7: The sputtering deposition schematic diagram of silver thin films in pure Ar and pure N_2 atmospheres.

proved by the cross-sectional morphology in Figure 5. Moreover, in Ar discharge, the high mobility and big size of Ag clusters lead to big initial grain size during the coalescence stage. During the grain growth, the lower mobility and diffusion leads to a higher nucleation rate in N_2 discharge. Therefore, the initial and final grain size in Ar discharge is bigger than that in N_2 discharge. In FCC metal, (111) plane has the lowest surface energy and (100) plane has the lowest strain energy [24]. The relative higher strain energy exists in silver thin films due to the fact that a lot of defects exist in loose-packed model of Ag clusters. Therefore, the competition between surface energy and strain energy is also responsible for the orientation evolution, which agreed with the mobility and diffusion results of Ag clusters. In conclusion, the N_2 content has a significant influence on the microstructures of silver thin films, and the grain boundary scattering and defect scattering caused by the microstructures of films are mainly responsible for the change in electrical properties.

4. Conclusions

The sputtering gas N_2 content plays an important role on microstructures of silver thin films during the deposition. As the N_2 content increases, Ag (111) preferred orientation is gradually evolved into (100) preferred orientation. When N_2 is more than 12.5 vol.%, silver thin films have highly (100) preferred orientation. The average grain size decreases from 82 nm to 31 nm as the N_2 content increases. Silver thin films exhibit low relative density when the N_2 content exceeds 33.3 vol.%. The mobility, diffusion, and energy of Ag clusters are mainly responsible for changes in the microstructures of silver thin films. The resistivity of silver thin films is altered with the changes of the microstructures in silver thin films. When the N_2 content ranges from 0 vol.% to 33.3 vol.%, the resistivity of silver thin films increases slightly, which is mainly the result of the grain boundary scattering. The defects scattering is mainly responsible for high resistivity of films prepared at high N_2 content. Based on the results of films' resistivity and microstructures, the optimum range of N_2 content to get compact silver thin films is below 33.3 vol.%.

Data Availability

All data used to support the findings of this study are included within the article.

Conflicts of Interest

The authors declare that there are no conflicts of interest regarding the publication of this paper.

Acknowledgments

This study was financially supported by the Foundation of National Key Laboratory, P R China (6142808180102) and National Natural Science Foundation of China (grant no. 51401080).

References

[1] E. Kudo, S. Hibiya, M. Kawamura et al., "Optical properties of highly stable silver thin films using different surface metal layers," *Thin Solid Films*, vol. 660, pp. 730–732, 2018.

[2] O. Baghriche, S. Rtimi, A. Zertal, C. Pulgarin, R. Sanjinés, and J. Kiwi, "Accelerated bacterial reduction on Ag-TaN compared with Ag-ZrN and Ag-TiN surfaces," *Applied Catalysis B: Environmental*, vol. 174-175, pp. 376–382, 2015.

[3] J. Zhu, Y. Hu, M. Xu et al., "Enhancement of the adhesive strength between Ag films and Mo substrate by Ag implanted via ion beam-assisted deposition," *Materials*, vol. 11, no. 5, p. 762, 2018.

[4] A. H. Aly, M. Ismail, and E. Abdel-Rahman, "Ag/GaN one dimensional photonic crystal for many applications," *Journal of Computational and Theoretical Nanoscience*, vol. 9, no. 4, pp. 592–596, 2012.

[5] J.-O. Song, J. Seop Kwak, Y. Park, and T.-Y. Seong, "Ohmic and degradation mechanisms of Ag contacts on p-type GaN," *Applied Physics Letters*, vol. 86, no. 6, Article ID 062104, 2005.

[6] L. Gao, J. Gstöttner, R. Emling et al., "Thermal stability of titanium nitride diffusion barrier films for advanced silver interconnects," *Microelectronic Engineering*, vol. 76, no. 1–4, pp. 76–81, 2004.

[7] L. Gao, J. Gstöttner, R. Emling et al., "Silver metallization with reactively sputtered TiN diffusion barrier films," *MRS Online Proceedings Library Archive*, vol. 812, 2004.

[8] S. Mardani, D. Primetzhofer, L. Liljeholm, Ö. Vallin, H. Norström, and J. Olsson, "Electrical properties of Ag/Ta and Ag/TaN thin-films," *Microelectronic Engineering*, vol. 120, pp. 257–261, 2014.

[9] S. Rtimi, O. Baghriche, R. Sanjines et al., "Photocatalysis/catalysis by innovative TiN and TiN-Ag surfaces inactivate bacteria under visible light," *Applied Catalysis B: Environmental*, vol. 123-124, pp. 306–315, 2012.

[10] M. Kawamura, K. Iibuchi, Y. Abe, and K. Sasaki, "Crystal orientation change of Ni films by sputtering in Ar-N_2 mixed gases," *Japanese Journal of Applied Physics*, vol. 43, no. 7A, pp. 4361-4362, 2004.

[11] M. Kawamura, K. Yagi, Y. Abe, and K. Sasaki, "Effects of the Ar-N_2 sputtering gas mixture on the preferential orientation of sputtered Ru films," *Thin Solid Films*, vol. 494, no. 1-2, pp. 240–243, 2006.

[12] R. Calinas, M. T. Vieira, and P. J. Ferreira, "The effect of nitrogen on the formation of nanocrystalline copper thin films," *Journal of Nanoscience and Nanotechnology*, vol. 9, no. 6, pp. 3921–3926, 2009.

[13] G. R. Sánchez, C. L. Castilla, N. B. Gómez, A. García, R. Marcos, and E. R. Carmona, "Leaf extract from the endemic plant Peumus boldus as an effective bioproduct for the green synthesis of silver nanoparticles," *Materials Letters*, vol. 183, pp. 255–260, 2016.

[14] M. S. Jee, H. S. Jeon, C. Kim et al., "Enhancement in carbon dioxide activity and stability on nanostructured silver electrode and the role of oxygen," *Applied Catalysis B: Environmental*, vol. 180, pp. 372–378, 2016.

[15] X. Gao, M. Hu, Y. Fu, L. Weng, W. Liu, and J. Sun, "Low temperature deposited Ag films exhibiting highly preferred orientations," *Materials Letters*, vol. 213, pp. 178–180, 2018.

[16] Y. Wang, W. Tang, and L. Zhang, "Crystalline size effects on texture coefficient, electrical and optical properties of sputter-deposited Ga-doped ZnO thin films," *Journal of Materials Science & Technology*, vol. 31, no. 2, pp. 175–181, 2015.

[17] E. H. Sondheimer, "The mean free path of electrons in metals," *Advances in Physics*, vol. 1, no. 1, pp. 1–42, 1952.

[18] P. P. Wang, X. J. Wang, J. L. Du et al., "The temperature and size effect on the electrical resistivity of Cu/V multilayer films," *Acta Materialia*, vol. 126, pp. 294–301, 2017.

[19] W. Zhang, S. H. Brongersma, O. Richard et al., "Influence of the electron mean free path on the resistivity of thin metal films," *Microelectronic Engineering*, vol. 76, no. 1–4, pp. 146–152, 2004.

[20] B. Fritsche, T. Chevolleau, J. Kourtev, A. Kolitsch, and W. Möller, "Plasma diagnostic of an RF magnetron Ar/N_2 discharge," *Vacuum*, vol. 69, no. 1–3, pp. 139–145, 2002.

[21] M. D. Logue and M. J. Kushner, "Electron energy distributions and electron impact source functions in Ar/N_2 inductively coupled plasmas using pulsed power," *Journal of Applied Physics*, vol. 117, no. 4, article 043301, 2015.

[22] P. G. Reyes, C. Torres, and H. Martínez, "Electron temperature and ion density measurements in a glow discharge of an Ar-N_2 mixture," *Radiation Effects and Defects in Solids*, vol. 169, no. 4, pp. 285–292, 2014.

[23] M. M. Mansour, N. M. El-Sayed, and O. F. Farag, "Effect of He and Ar addition on N_2 glow discharge characteristics and plasma diagnostics," *Arab Journal of Nuclear Sciences and Applications*, vol. 46, no. 1, pp. 116–125, 2013.

[24] J.-M. Zhang, Y. Zhang, and K.-W. Xu, "Dependence of stresses and strain energies on grain orientations in FCC metal films," *Journal of Crystal Growth*, vol. 285, no. 3, pp. 427–435, 2005.